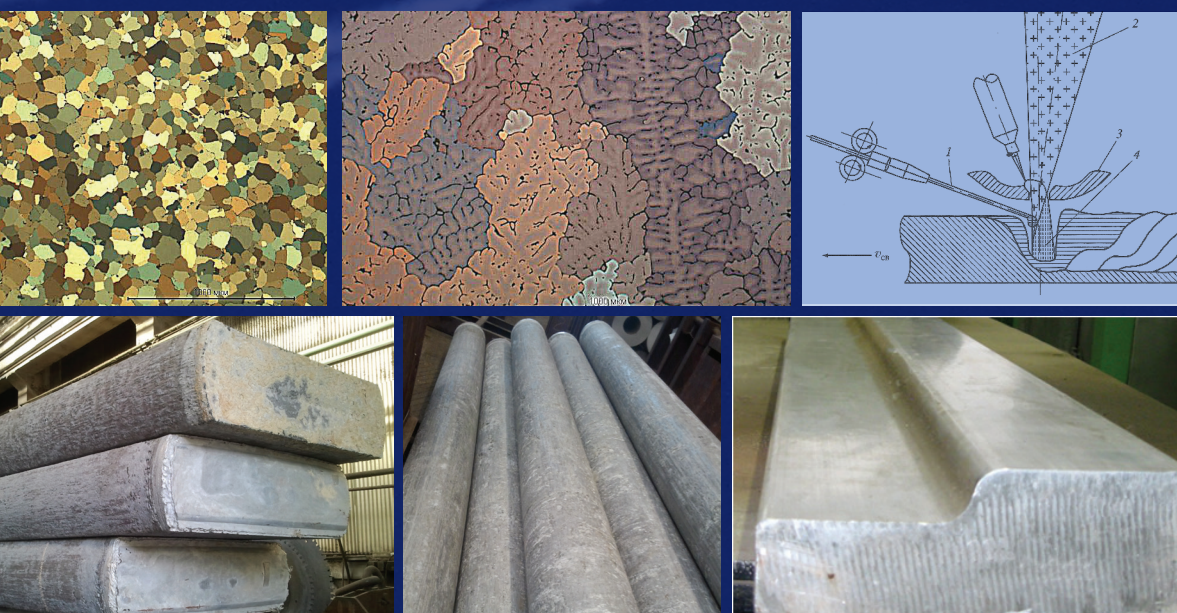


**ADVANCES IN METALLIC ALLOYS**

A series edited by D. G. Eskin

# ALUMINUM–LITHIUM ALLOYS

Process Metallurgy,  
Physical Metallurgy,  
and Welding



**Olga Grushko**  
**Boris Ovsyannikov**  
**Viktor Ovchinnikov**



CRC Press  
Taylor & Francis Group

# ALUMINUM–LITHIUM ALLOYS

Process Metallurgy, Physical  
Metallurgy, and Welding

# Advances in Metallic Alloys

A series edited by **D.G. Eskin**, *Brunel Centre for Advanced Solidification Technology (BCAST), Brunel University*

---

## **Volume 1**

Liquid Metal Processing: Applications to Aluminum Alloy Production  
*I.G. Brodova, P.S. Popel and G.I. Eskin*

## **Volume 2**

Iron in Aluminum Alloys: Impurity and Alloying Element  
*N.W. Belov, A.A. Aksenov and D.G. Eskin*

## **Volume 3**

Magnesium Alloy Containing Rare Earth Metals: Structure and Properties  
*L.L. Rokhlin*

## **Volume 4**

Phase Transformations of Elements Under High Pressure  
*E.Yu Tonkov and E.G. Ponyatovsky*

## **Volume 5**

Titanium Alloys: Russian Aircraft and Aerospace Applications  
*Valentin N. Moiseyev*

## **Volume 6**

Physical Metallurgy of Direct Chill Casting of Aluminum Alloys  
*Dmitry G. Eskin*

## **Volume 7**

Ultrasonic Treatment of Light Alloy Melts, Second Edition  
*Georgy I. Eskin and Dmitry G. Eskin*

## **Volume 8**

Aluminum–Lithium Alloys: Process Metallurgy, Physical Metallurgy,  
and Welding  
*Olga Grushko, Boris Ovsyannikov, and Viktor Ovchinnikov*

# ALUMINUM–LITHIUM ALLOYS

Process Metallurgy, Physical  
Metallurgy, and Welding

**Olga Grushko**  
**Boris Ovsyannikov**  
**Viktor Ovchinnikov**



**CRC Press**

Taylor & Francis Group

Boca Raton London New York

---

CRC Press is an imprint of the  
Taylor & Francis Group, an **informa** business

CRC Press  
Taylor & Francis Group  
6000 Broken Sound Parkway NW, Suite 300  
Boca Raton, FL 33487-2742

© 2017 by Taylor & Francis Group, LLC  
CRC Press is an imprint of Taylor & Francis Group, an Informa business

No claim to original U.S. Government works

Printed on acid-free paper  
Version Date: 20160708

International Standard Book Number-13: 978-1-4987-3717-3 (Hardback)

This book contains information obtained from authentic and highly regarded sources. Reasonable efforts have been made to publish reliable data and information, but the author and publisher cannot assume responsibility for the validity of all materials or the consequences of their use. The authors and publishers have attempted to trace the copyright holders of all material reproduced in this publication and apologize to copyright holders if permission to publish in this form has not been obtained. If any copyright material has not been acknowledged please write and let us know so we may rectify in any future reprint.

Except as permitted under U.S. Copyright Law, no part of this book may be reprinted, reproduced, transmitted, or utilized in any form by any electronic, mechanical, or other means, now known or hereafter invented, including photocopying, microfilming, and recording, or in any information storage or retrieval system, without written permission from the publishers.

For permission to photocopy or use material electronically from this work, please access [www.copyright.com](http://www.copyright.com) (<http://www.copyright.com/>) or contact the Copyright Clearance Center, Inc. (CCC), 222 Rosewood Drive, Danvers, MA 01923, 978-750-8400. CCC is a not-for-profit organization that provides licenses and registration for a variety of users. For organizations that have been granted a photocopy license by the CCC, a separate system of payment has been arranged.

**Trademark Notice:** Product or corporate names may be trademarks or registered trademarks, and are used only for identification and explanation without intent to infringe.

---

#### Library of Congress Cataloging-in-Publication Data

---

Names: Grushko, Olga, author. | Ovsyannikov, Boris, author. | Ovchinnikov, Viktor, author.  
Title: Aluminum-lithium alloys : process metallurgy, physical metallurgy, and welding / authors, Olga Grushko, Boris Ovsyannikov, and Viktor Ovchinnikov.  
Description: Boca Raton : Taylor & Francis, CRC Press, 2017. | Series: Advances in metallic alloys ; volume 8 | Includes bibliographical references and index.  
Identifiers: LCCN 2016006752 | ISBN 9781498737173 (hardcover : alk. paper)  
Subjects: LCSH: Aluminum-lithium alloys--Metallurgy.  
Classification: LCC TN775 .G745 2017 | DDC 669/.722--dc23  
LC record available at <https://lccn.loc.gov/2016006752>

---

Visit the Taylor & Francis Web site at  
<http://www.taylorandfrancis.com>

and the CRC Press Web site at  
<http://www.crcpress.com>

---

# Contents

Authors.....	ix
Introduction.....	xi
<b>Chapter 1</b> Brief History of Aluminum–Lithium Alloy Creation.....	1
<b>Chapter 2</b> Theoretical Basis of Aluminum–Lithium Alloying with Controlled Lithium Content and Metallic and Nonmetallic Impurities .....	11
2.1 Kinetics of Aluminum Alloy Oxidation in Molten Condition .....	11
2.2 Oxidation Kinetics and Mechanism of Protective Alloying of Aluminum–Lithium Alloys .....	16
2.2.1 Al–Cu–Li System Alloy .....	16
2.2.2 Al–Mg–Li System Alloy .....	17
2.3 Thermodynamics of Molten Aluminum: Flux System .....	23
2.4 Selection of Inert and Protective Atmospheres .....	26
2.5 Nonmetallic Impurities and Alkali and Alkaline-Earth Element Impurities in Aluminum–Lithium Alloys.....	27
2.5.1 Oxygen, Nitrogen, and Carbon in the 1420 Alloy.....	27
2.5.2 Alkali and Alkaline-Earth Element Impurities in Aluminum–Lithium Alloys.....	30
2.5.3 Interaction of Aluminum–Lithium Alloy with the Lining Material .....	34
<b>Chapter 3</b> Hydrogen in Aluminum–Lithium Alloys.....	37
3.1 Interaction of Aluminum Alloys with Hydrogen .....	37
3.2 Changing of Hydrogen Content in Aluminum–Lithium Alloys Depending on the Conditions of Melting.....	40
3.2.1 Sources of Hydrogen in Aluminum–Lithium Alloys .....	41
3.2.2 Hydrogen in 1420 Alloy during Melting in Reverberatory Furnace.....	43
3.2.3 Effectiveness of Vacuuming of Aluminum–Lithium Alloys .....	46
3.2.4 Electroflux Refining of Aluminum–Lithium Alloys .....	49
3.2.5 Nature of Hydrogen Distribution in 1420 Alloy Billets and Semi-Finished Products .....	51
3.3 About Forms of Hydrogen Presence in Lithium-Aluminum Alloys.....	55

<b>Chapter 4</b>	Crack Susceptibility and Peculiarities of Casting Aluminum–Lithium Alloy Billets.....	63
4.1	Casting Crack Susceptibility Depending on Chemical Composition .....	63
4.1.1	Cold Cracks .....	64
4.1.2	Hot Cracks.....	71
4.2	Peculiarities of Casting Billets from Aluminum–Lithium Alloys.....	82
4.2.1	Necessity of Melt Protection against Exposure to Shop Atmosphere .....	82
4.2.2	Practical Realization of the Technology Developed .....	84
<b>Chapter 5</b>	Aluminum–Lithium Alloy Grain Structure Solidification Conditions and Peculiarities .....	89
5.1	Ingot Heat Conductivity Properties and Solidification Conditions.....	89
5.1.1	Cylinder Billet Solidification.....	91
5.1.2	Flat Ingot Solidification.....	96
5.2	Conditions for the Generation of Zones with Variable Etchability in Aluminum–Lithium Alloys and Zone Influence on Semifinished Product Properties .....	102
5.3	Grain Structure of Slabs of Aluminum Alloys Doped with Lithium .....	109
5.4	Principle of Nondendritic Structure Formation in Aluminum Alloy Slabs Avoiding Physical Influence on Solidifying Metal.....	116
5.5	Hereditary Influence of Slab Grain Structure on Slab Flow Characteristics .....	119
<b>Chapter 6</b>	Excess Hetero-Phase in 1420 Alloy Billets and Its Hereditary Influence on the Structure, Properties, and Weldability of Semifinished Products.....	123
6.1	Phases Formed by the Main Alloying Agents and Controlled Additives Traditional for Aluminum Alloys .....	123
6.2	Alkaline and Alkaline-Earth Elements in Aluminum–Lithium Alloys.....	135
6.2.1	Phases Formed by Calcium and Barium in 1420 Alloy Industrial Billets.....	138
6.2.2	The Influence of Sodium, Calcium, and Barium Impurities Individually and Collectively within the Actually Existing Industrial Concentration Melts on Structure and Properties of Experimental Billets and Forgings.....	140

	6.2.2.1	Test Procedure .....	140
	6.2.2.2	Billet Structure and Properties .....	142
	6.2.2.3	Forging Structure and Properties .....	148
6.2.3		Nature of Relationship between 1420 Alloy Properties and Alkaline and Alkaline-Earth Metal Additives Concentration at Different Initial Purity of Burden Materials.....	148
	6.2.3.1	Preparation and the Experimental Procedure .....	148
	6.2.3.2	Billets and Forgings Properties .....	149
6.2.4		Sodium Behavior Peculiarities in Lithium Alloys .....	172
<b>Chapter 7</b>		<b>Structure, Mechanical Properties, and Weldability of Alloy 1420 Die Forgings of Complicated Configuration versus Initial Slab Structure and Pressure-Forming Modes .....</b>	<b>175</b>
7.1		Principle of Structure Defect Development in Aluminum Alloys in Semifinished Products.....	177
7.2		Pressure-Forming Modes versus the Structure, Properties, and Weldability of Alloy 1420 Forgings .....	179
	7.2.1	Forging and Weld Seam Structure and Mechanical Properties.....	179
	7.2.2	Tendency toward Opening at Ingot and Forging Hot Tests .....	181
	7.2.3	Forging Structure Formation Principle versus Forming Mode.....	183
7.3		Comparative Study of Structure and Mechanical Properties of Massive Alloy 1420 Die Forgings Produced per Various Forming Modes.....	189
7.4		Alloy 1420 Massive Die Forging Properties and Weldability versus Manufacturing Process Parameters and Structure .....	192
	7.4.1	Die Forging Properties versus Melt Preparation Method.....	192
	7.4.2	Analysis of Weld Seams at Die Forgings .....	193
	7.4.2.1	Defects Dependent on the Hydrogen Content in the Base Metal and Semifinished Product Structure.....	194
	7.4.2.2	Defects Associated with Welding Conditions .....	212
<b>Chapter 8</b>		<b>Aluminum–Lithium Alloy Welding Process Features.....</b>	<b>219</b>
8.1		Aluminum–Lithium Alloy Electric Resistance Welding .....	219
8.2		Aluminum–Lithium Sheet Semifinished Product Fusion Welding Features .....	224

8.3	Wire-Filler Selection for Aluminum–Lithium Alloy Sheets Arc Welding .....	230
8.4	Welding Method versus Aluminum–Lithium Alloy Welded Joints Properties .....	233
8.5	Transformations at Heat Influence Zone at Aluminum–Lithium Alloy Welding Process .....	246
8.6	Aluminum–Lithium Alloy Laser Beam Welding Process Features .....	249
8.7	Aluminum–Lithium Alloy Friction Stir Welding Features.....	256
8.8	Weld Backups versus Aluminum–Lithium Alloy Welded Joints Properties .....	264
8.9	Aluminum–Lithium Alloy Multipass Welding .....	266
8.10	Aluminum–Lithium Alloy Electron Beam Welding.....	271
	Conclusions .....	285
	References .....	287
	<b>Index</b> .....	<b>301</b>

---

# Authors

**Dr. Sci. Olga Grushko** graduated from Moscow State Aviation Technological University in 1959. She specializes in metallurgy and materials science for wrought aluminum alloys. Since 1959, she has been working at the All-Russian Research Institute of Aviation Materials (VIAM) and, in recent years, as a chief scientist.

Dr. Grushko is well known for the fundamental development of a new wrought aluminum alloys class—alloys with lithium. Her theoretical ideas and research are implemented in industrial production.

Dr. Grushko is the author of 90 publications and 20 inventions, a doctor of engineering sciences, and a recipient of a State Award from the Russian Federation for the development new lightweight alloys.

**Dr. Boris Ovsyannikov** graduated from Ural Federal University in 1979. He is a specialist in the field of melting, casting, and metallurgy of aluminum and magnesium wrought alloys, and the technology of rare metals. Since 1984, he has been working at Kamensk-Uralsky Metallurgical Works. He became chief metallurgist in 2011 and head of R&D in 2014.

Dr. Ovsyannikov developed the scientific basis for melting, refining, and casting of aluminum alloys alloyed with lithium and rare earth metals. His theoretical developments are implemented in the industrial production of ingots in aluminum alloys alloyed with lithium and scandium.

Dr. Ovsyannikov is the author of 95 publications and 28 inventions. He holds a PhD in casting production engineering.

**Prof. Dr. Sci. Viktor Ovchinnikov** graduated from Moscow Aviation Technological Institute in 1978. He specializes in metallurgy and welding of wrought aluminum alloys. Since 1982, he has been working at the Russian Aircraft Corporation JSC and is head of the Welding Laboratory.

Prof. Ovchinnikov developed a scientific basis for fusion welding of aluminum–lithium alloys and methods for the prevention of porosity in joints. He has implemented theoretical and practical developments in the manufacturing of welded aircraft structures.

Prof. Ovchinnikov is the author of 470 publications and 110 inventions. He is a doctor of engineering sciences, professor, full member of the International Informatics Academy, and has received an award for excellent invention in the aviation industry.



# Taylor & Francis

Taylor & Francis Group

<http://taylorandfrancis.com>

---

# Introduction

Starting with the introduction of the first aluminum–lithium alloys and throughout their mastering and implementation into structures, there have been activities toward developing scientific fundamentals and practical realizations of technological processes and equipment for ingot melting and casting, production of a wide range of semifinished products with the guaranteed chemical composition, structure, and complexity of performance characteristics, and also welding modes by production of welded parts. In parallel with the development of new alloys, the compositions of older alloys have been improved in the process of mastering and enhancing their processibility and reliability characteristics.

This book summarizes the results of work since the 1960s to solve problems with melting, ingot casting, and producing massive forged semifinished products for welded parts in the welding of aluminum–lithium alloys.

The history of the creation of aluminum–lithium alloys and primary areas of their application in aircraft structures are briefly presented in [Chapter 1](#).

[Chapter 2](#) details matters of oxidation kinetics and a mechanism for protective alloying of aluminum–lithium alloys, a selection of fluxes and inert protective atmospheres, and the interaction of aluminum–lithium melt with lining materials.

[Chapter 3](#) is devoted to the consideration of sources of melt enrichment with hydrogen, hydrogen distribution in aluminum–lithium alloy ingots, and a study of the presence of hydrogen in aluminum–lithium alloys.

[Chapter 4](#) covers the influence of chemical composition of the alloy and its susceptibility on casting cracking. It deals with peculiarities of casting ingots in aluminum alloys doped with lithium, and represents a practical realization of the developed technology of ingot casting.

A mechanism of nondendritic structure formation in aluminum alloy ingots without any physical effect to the solidifying metal, and a hereditary influence of grain-typed structure of ingots on their rheological characteristics are discussed in [Chapter 5](#).

[Chapter 6](#) is devoted to excess heterophasicity in 1420 alloy ingots and its hereditary influence on the structure and properties of semifinished products.

The peculiarities of modern aluminum–lithium welding and the structure and tensile properties of welded joints are reviewed in [Chapter 7](#). A mechanism of welded joint structure formation on massive forgings in alloy 1420 is also presented.

[Chapter 8](#) details matters of aluminum–alloy weldability, tensile properties, and structure of welded joints. All modern techniques of producing aluminum–lithium seams on semifinished products of a wide thickness range are described.

The authors trust that this book will be useful for engineers and scientists involved in the research, development, and implementation of welded structures in high-strength aluminum alloys.



# Taylor & Francis

Taylor & Francis Group

<http://taylorandfrancis.com>

---

# 1 Brief History of Aluminum–Lithium Alloy Creation

The creation of new generations of civil and combat aircraft, and leading-edge design solutions for aerospace engineering, requires industrial production development and mastering of new structural materials and new design solutions and processes for their usage in parts. The basic structural materials in civil aircraft are aluminum alloys, but they are also used on a large scale in structures of other aircraft types. In Russia and abroad, research is being carried out toward the development of aluminum alloys to ensure maximum weight efficiency. One of the ways to address this is the development of reduced-density alloy compositions.

Researchers have turned their attention to lithium, which has a unit weight of  $0.536 \text{ MT m}^{-3}$ . The first alloys appeared in the 1950s and were based on the Al–Cu–Li system, such as the alloys X2020 (USA) and VAD23 (USSR), later known as 1230. These alloys were 3% lighter and 8% harder than conventional alloys 2024 and D16; also, they demonstrated high strength at room and elevated temperatures (up to  $175^\circ\text{C}$ ). The alloy X2020 used in the design of military seaborne airplane served, as mass media reported, for many years without complaints. The alloy VAD23 in the form of thin cross-sectional profiles was part of the design of the supersonic commercial airliner TU144, but that program was withdrawn. Nevertheless, due to its high elasticity modulus, VAD23 (1230) was used in a number of reconditioned parts where sheets were produced in considerable quantities through to the 1990s.

The genuine breakthrough in the development of lithium-doped aluminum (Al–Li) alloys was made by a team of VIAM scientists (V. F. Shamrai, N. V. Shiryaeva) supervised by academician I. N. Fridlyander: the invention of the hardening effect by heat treating an extensive group of alloys in the ternary Al–Mg–Li system [1]. At the same time, it was determined that lithium with an elasticity modulus smaller than that of aluminum increased the elasticity modulus of the alloys from the Al–Mg–Li system by up to 8%. That effect was marked as an invention (the “Fridlyander effect”) [1].

Based on that system, the lightest aluminum alloy 1420 containing 2% lithium and 5.5% magnesium [2] was offered. Two percent of lithium by weight is equivalent to 11 at.% of aluminum alloy. Therefore, alloy 1420 is 10%–12% lighter than duralumin-type alloys used for the fuselage with the same strength characteristics; moreover, it has high corrosion resistance.

Between 1970 and 1971, the serial production of vertical takeoff and landing (VTOL) jets Yak-36 and Yak-38 was started, with riveted fuselages made of



**FIGURE 1.1** Yak-38 fighter, where alloy 1420 was used (first serial utilization of the Al–Li alloy).

alloy 1420, which were based onboard and inboard sea aircraft carriers (Figure 1.1). Even after many years of their operation, there were problems reported due to alloy 1420. The fighter Yak-36 is being successfully operated even today [3]. The application of alloy 1420 in the riveted structure resulted in weight reduction by 16%.

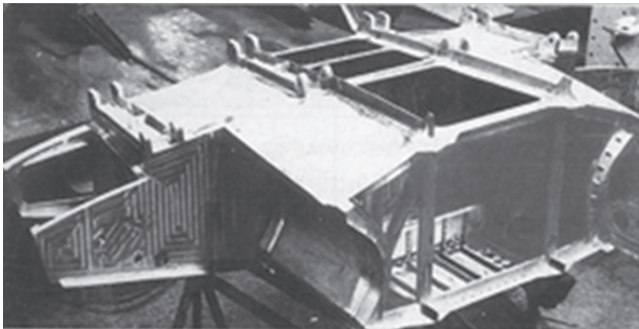
Successful application of alloy 1420 gave rise to the active development of Al–Li alloys and drew the design engineers’ attention to the use of these alloys. In the 1980s and 1990s, both in Russia (Soviet Union) and other countries, alloys were developed based on Al–Li–Cu and Al–Li–Mg–Cu systems, but work was in progress in Russia to create new alloys based on the Al–Li–Mg system as well. All Al–Li alloys were additionally doped with zirconium and manganese. Calcium was introduced into alloy 1420 as an alloying element.

In Russia, scandium is widely used to dope Al–Li alloys (alloys 1421, 1461, 1424, B-1461, V-1464, V-1469). Western companies have started using silver for doping (alloys 2094, 2095, 2195, 2196, and 2098) since 1990. In Russia, alloy V-1469 became the first to contain silver. After 2012, Western companies registered Al–Li alloys with zinc (2397, 2099); at the same time, alloys with zinc (1424, B-1461) appeared in Russia.

In 1985, the A. I. Mikoyan Design Bureau, upon the initiative of M. R. Valdenberg, deputy chief designer, started work to create a welded airplane using aluminum. For the first time in the world, a welded fuselage of one of the MiG-29 fighter modifications was made in aluminum alloy 1420 [3]. A large variety of semifinished products—more than 150 items of forgings, extruded panels, and sheets—were used in the design. They were also used to fabricate leakproof, welded fuel tanks, and cockpits (Figure 1.2), which resulted in weight reduction of the design elements by up to 27%.



(a)



(b)

**FIGURE 1.2** (a) MiG-29M fighter, where welded structures in Al–Li alloy 1420 were used, (b) fuel tank.

MiG-29 aircraft with welded tanks made of alloy 1420 are in service even today. That work evolved during the creation of the welded structure of the new-generation fighter 1–44 [3–5].

There are up to 800 sheet-formed parts in alloy 1420 used in the unloaded areas of the fighter-interceptor Su-27 (1985) (Figure 1.3).

Welded hulls of submarine-launched missiles are manufactured from alloy 1420, and then from its modification 1421. Alloy 1420 is being used in the structure of a number of other similar parts [3] for many years.

With the purpose of reducing the weight of parts, the G. M. Beriev Aircraft Company took a decision to use 1441 alloy sheets in the Be-200 and Be-103 programs. Alloy 1441 is rolled well in both clad and bare forms, which allows producing thin sheets (up to 1.2 mm) by coil rolling. Alloy sheets with the same strength characteristics have a higher fatigue crack growth resistance and a longer life than 1163AT alloy sheets by a factor of 1.5 (Figure 1.4) [6,7].



**FIGURE 1.3** Su-27 fighter interceptor.

At the end of the 1980s, the Antonov Design Bureau started trials with a new lithium-containing alloy, 1450, for their transport aircraft programs. The Bureau developed the world's largest airplanes "Ruslan" and "Mria"; therefore, ingots with a cross section of  $400 \times 1450$  and  $450 \times 1200$  mm were cast to manufacture large plates and extruded panels, which were used in those planes [8] (Figure 1.5).

In 1995, A. N. Tupolev ANTK, after evaluating data on alloy 1420's properties and applications in the military aircraft programs Yak-36, Yak-38, and MiG-29, took a decision to use the Al–Li alloy 1420 in the civil airplane Tu-204 for the first time. It was used for nonweight-bearing structures such as sheets (fuselage stringer set, fillets, compensators), extruded profiles (floor beam ribs and walls, interior element fixtures, equipment location racks), and die-forgings (manhole covers, reinforcement elements).

With the substitution of parts made of alloy 1163, a weight reduction of 10%–12% was achieved. The possibilities for applying alloy 1420 die-forgings as window frames are being worked out.

Also, a number of similar parts for a new short- to medium-range commercial airplane, Tu-334 (2003), are also made using alloy 1420.

A number of parts for the experimental airplane Tu-156 with an LNG- and kerosene-fired engine were fabricated using alloy 1420. The use of alloy 1460 (new modification is 1461) to manufacture tanks for cryogenic propellants was reviewed for Tu-156 and a cryogen-powered plane [9,10]. A welded tank was manufactured using this alloy and successfully tested for the McDonnell Douglas Reusable Launch Vehicle. Alloy 1460 was used to substitute alloy 1201, which resulted in a welded tank weight reduction by up to 25%.

In 2003, the strongest corrosion-resistant weldable alloy V-1469 was developed based on the Al–Cu–Li–Mg system doped with zirconium, scandium, and silver [11,12]. The alloy has extremely high processibility by metal forming, which allows producing sheets with 1.5 mm thickness, cold-rolled coils, rolled rings, and extruded



(a)



(b)

**FIGURE 1.4** (a) Be-200 hydroplane and (b) Be-103 hydroplane, where Al–Li alloy sheets were used in their design.



**FIGURE 1.5** World’s largest transport airplane “Mria,” where semifinished products in Al–Li alloys were used, including large extruded panels in alloy 1450.

profiles of various cross sections. Also, sheets with thickness down to 0.35 mm were produced [12]. The alloy is recommended for use in the MC21 design and also for welded tanks for cryogenic propellants.

Numerous researches have demonstrated the potential of Al–Li alloys in superplastic forming [13–18]. In the 1980s, OAO KUMZ manufactured and supplied sheets made of alloy 1420RS with the specified grain size for superplastic forming to their customers. Parts of complex configuration were formed from the sheets.

To obtain semifinished products in Al–Li alloys in the industrial metallurgical production environment during process development, there was a challenge to overcome the formidable tasks associated with the presence of lithium in the alloys [3,22].

First of all, lithium is extremely chemically active in molten aluminum, which requires protecting the melt surface at all stages of technological processes subject to liquid phase existence (melting, ingot casting, fusion welding) from lithium losses and saturation with hydrogen. During the production of clad sheets, due to their high oxidizability at rolling temperatures, special preparation of their surface is also required [20,21].

Second, alloys with lithium have higher elasticity modulus and lower heat conductivity. Therefore, temperature gradients during ingot casting and forming result in the buildup of stresses higher than in conventional aluminum alloys without lithium.

Third, alloys of the Al–Mg–Li system have a tendency to localize strains, which complicates the generation of the specified structure and properties in massive short-transverse cross sections and also sheet hardening by cold rolling. The latter does not allow the production of sheets by cold coil rolling [19].

Starting from the development of first the Al–Li alloys and throughout the period of their mastering and implementation into designs, work was in progress to develop technological processes and equipment for melting and ingot casting, produce a wide range of semifinished products with the guaranteed chemical composition and structure, obtain a complete set of performance characteristics, and also develop welding modes by production of welded parts. In addition to the development of new alloys within the mastering process, improvements were made in the compositions of previously developed alloys to enhance their processibility and reliability characteristics [23–26, 119–123].

Russian and foreign researchers developed a broad range of alloys, whose compositions are given in [Tables 1.1](#) and [1.2](#).

This book summarizes the results of the work on resolving problems of melting, ingot casting, production of massive hammered and forged semifinished products for welded parts, and issues of Al–Li alloy welding performed from the 1960s up to now, in which the authors were directly involved.

Invaluable contributions to the development of Al–Li alloys were made by the following Russian scientists and industrial specialists: V.M. Baranchikov, N.D. Vinokurov, G.D. Volkhin, I.Ya. Zaltsman, V.A. Zasyepkin, L.A. Ivanova, E.N. Kablov, V.G. Kovalyov, L.V. Kuzmichev, K.N. Mikhaylov, I.I. Novikov, A.E. Semyonov, O.A. Setyukov, V.M. Chertovikov, S.B. Komarov, V.I. Popov, V.E. Anfyorov, V.I. Blagodatskikh, and S.M. Mozharovskiy (melting, casting, rolling processes);

**TABLE 1.1**  
**Russian Aluminum–Lithium Alloys**

Alloy	Element Percentage by Weight (%)												Others		Al
	Si	Fe	Cu	Mn	Mg	Cr	Zn	Ti	Ni	Li	Zr	Other Elements	Each	Total	
	1420	0.15	0.2	0.05	—	4.5–6.0	—	—	0.1	—	1.8–2.2	0.08–0.15	Be: 0.0002–0.005 Ca: 0.04 Na: 0.03 (0.0015 <sup>a</sup> )	0.05	
1421	0.2	0.2	—	—	4.5–5.3	—	—	0.1	—	1.8–2.2	0.06–0.10	Be: 0.03 Sc: 0.16–0.21 Na: 0.005	0.05	0.15	Base
1430	0.1	0.15	1.4–1.8	0.25	2.3–3.0	—	—	0.01–0.1	—	1.5–1.9	0.08–0.14	Be: 0.02–0.1 Sc: 0.01–0.1 Na: 0.003	0.05	0.15	Base
1440	0.02–0.1	0.03–0.15	1.2–1.9	0.05	0.6–1.1	0.05	0.1	0.02–0.1	—	2.1–2.6	0.10–0.2	Be: 0.05–0.2 Na: 0.003	0.05	0.15	Base
1441	0.08	0.12	1.5–1.8	0.001–0.10	0.7–1.1	—	—	0.01–0.07	0.02–0.10	1.8–2.1	0.04–0.16	Be: 0.02–0.20	0.05	0.15	Base
1450	0.1	0.15	2.6–3.3	0.1	0.1	0.05	0.25	0.01–0.06	—	1.8–2.3	0.08–0.14	Be: 0.008–0.1 Na: 0.002 Ce: 0.005–0.05	0.05	0.15	Base
1460	0.1	0.03–0.15	2.6–3.3	—	0.05	—	—	0.01–0.05	—	2.0–2.4	0.08–0.13	Na: 0.002 Ce: 0.005–0.03 Sc: 0.05–0.14 B: 0.0002–0.003	0.05	0.15	Base
1424	0.08	0.1	—	0.1–0.25	4.7–5.2	—	0.4–0.7	—	—	1.5–1.8	0.07–0.1	Be: 0.02–0.2 Sc: 0.05–0.08 Na: 0.0015	0.05	0.15	Base
1230 VAD23	0.3	0.3	4.8–5.8	0.4–0.8	0.05	—	0.1	0.15	—	0.9–1.4	—	Cd: 0.1–0.25	0.05	0.15	Base

(Continued)

**TABLE 1.1 (Continued)**  
**Russian Aluminum–Lithium Alloys**

Alloy	Element Percentage by Weight (%)												Others		Al
	Si	Fe	Cu	Mn	Mg	Cr	Zn	Ti	Ni	Li	Zr	Other Elements	Each	Total	
V-1461	0.08	0.01–0.1	2.5–2.95	0.2–0.6	0.05–0.6	0.01–0.05	0.2–0.8	0.05	0.05–0.15	1.5–1.95	0.05–0.12	Be: 0.0001–0.02 Sc: 0.05–0.10 Ca: 0.001–0.05 Na: 0.0015	0.05	0.10	Base
V-1469	0.1	0.12	3.2–4.5	0.003–0.5	0.1–0.5	—	—	—	—	1.0–1.5	0.04–0.20	Sc: 0.04–0.15 Ag: 0.15–0.6	0.05	0.10	Base
V-1464	0.03–0.08	0.03–0.10	3.25–3.45	0.20–0.30	0.35–0.45	—	—	0.01–0.03	—	1.55–1.70	0.08–0.10	Sc: 0.08–0.10 Be: 0.0003–0.002 Na: 0.0005	0.05	0.10	Base
1430	0.1	0.15	1.4–1.8	0.3–0.5	2.3–3.0	—	0.5–0.7	0.01–0.1	—	1.5–1.9	0.08–0.14	Be: 0.02–0.1 Sc: 0.01–0.1 Na: 0.003 Ce: 0.2–0.4 Y: 0.05–0.1	0.05	0.15	Base
1441K	0.08	0.12	1.3–1.5	0.001–0.10	0.7–1.1	—	—	0.01–0.07	0.01–0.15	1.8–2.1	0.04–0.16	Be: 0.002–0.01	0.05	0.15	Base
1445	0.08	0.12	1.3–1.8	0.001–0.10	0.7–1.1	—	—	0.01–0.1	0.01–0.15	1.6–1.9	0.04–0.16	Be: 0.002–0.01 Sc: 0.005–0.001 Ag: 0.05–0.15 Ca: 0.005–0.04 Na: 0.0015	0.05	0.15	Base

<sup>a</sup> For welded parts.

**TABLE 1.2**  
**Composition of Aluminum–Lithium Alloys Registered in the United States, France, and Great Britain**

Alloy	Registration Date	Si	Fe	Cu	Mn	Mg	Cr	Zn	Ti	Ag	Li	Zr	Others	
													Each	Total
2090	06.08.1984	0.10	0.12	2.4–3.0		0.25	0.05	0.10	0.15		1.9–2.6	0.08–0.15	0.05	0.15
2091	03.08.1985	0.20		1.8–2.5	0.10	1.1–1.9	0.10	0.25	0.10		1.7–2.3	0.04–0.16	0.05	0.15
2094	04.06.1990	0.12	0.15	4.4–5.2	0.25	0.25–0.8	—	0.25	0.10	0.25–0.6	0.7–1.4	0.04–0.18	0.05	0.15
2095	04.06.1990	0.12	0.15	3.9–4.6	0.25	0.25–0.8	—	0.25	0.10	0.25–0.6	0.7–1.5	0.08–0.16	0.05	0.15
2195	20.11.1992	0.12	0.15	3.7–4.3	0.25	0.25–0.8	—	0.25	0.10	0.25–0.6	0.8–1.2	0.04–0.18	0.05	0.15
2196	08.12.2000	0.12	0.15	2.5–3.3	0.35	0.25–0.8	—	0.35	0.10	0.25–0.6	1.4–2.1	0.08–0.16	0.05	0.15
2097	30.06.1993	0.12	0.15	2.5–3.1	0.10–0.6	0.35	—	0.35	0.15	—	1.2–1.8	0.08–0.15	0.05	0.15
2197	21.09.1993	0.10	0.10	2.5–3.1	0.10–0.50	0.25	—	0.05	0.12	—	1.3–1.7	0.08–0.15	0.05	0.15
2297	18.08.1997	0.10	0.10	2.5–3.1	0.10–0.50	0.25	—	0.05	0.12	—	1.1–1.7	0.08–0.15	0.05	0.15
2397	03.04.2002	0.10	0.10	2.5–3.1	0.10–0.50	0.25	—	0.05–0.15	0.12		1.1–1.7	0.08–0.15	0.05	0.15
2098	22.06.2000	0.12	0.15	2.3–3.8	0.35	0.25–0.8	—	0.35	0.10	0.25–0.6	2.4–2.8	0.04–0.18	0.05	0.15
2099	22.08.2003	0.05	0.07	2.4–3.0	0.10–0.50	0.10–0.50	—	0.40–1.0	0.10	—	1.6–2.0	0.08–0.12	0.05	0.15
8090	16.07.1984	0.20	0.30	1.0–1.6	0.10	0.6–1.3	0.10	0.25	0.10	—	2.2–2.7	0.04–0.16	0.05	0.15
8091	29.03.1985	0.30	0.50	1.0–1.6	0.10	0.50–1.2	0.10	0.25	0.10	—	2.4–2.8	0.08–0.16	0.05	0.15
8093	01.02.1990	0.10	0.10	1.6–2.2	0.10	0.9–1.6	0.10	0.25	0.10	—	1.9–2.6	0.04–0.14	0.05	0.15
8025	15.09.2000	0.05	0.06–0.25	0.20		0.05	0.18	0.50	0.005–0.02	—	3.4–4.2	0.08–0.25	0.05	0.15

S.M. Basyuk, N.F. Bulgakov, A.N. Gribkov, I.P. Zhegina, V.I. Zyryanov, S.I. Kishkina, L.V. Tarasenko, N.I. Turkina, A.A. Shadskiy, L.M. Shevelyova, and G.L. Shneider (hammering-forging, heat treating, and metallurgy); and V.V. Alekseev, Yu.P. Arbuzov, V.A. Varganov, V.B. Verdenskiy, V.V. Grinin, A.V. Gerasimenko, B.S. Denisov, L.F. Ermakov, E.N. Ioda, A.Ya. Ishchenko, A.I. Lopatkin, V.I. Lukin, A.I. Meylakh, A.V. Petrov, N.G. Tretyak, and V.I. Ryazantsev (welding).

---

# 2 Theoretical Basis of Aluminum–Lithium Alloying with Controlled Lithium Content and Metallic and Nonmetallic Impurities

## 2.1 KINETICS OF ALUMINUM ALLOY OXIDATION IN MOLTEN CONDITION

Aluminum and its alloys react with the ambient atmosphere during melting and casting. It is found that aluminum and aluminum alloy components can interact with hydrogen, nitrogen, water vapor, carbon monoxide (CO), and carbon dioxide (CO<sub>2</sub>) [27–29]. In small quantities, there are hydrogen and oxides in alloy, which have a significant influence on metal properties. At the beginning of this study in 1960, there were no systematic data on the behavior of lithium-containing aluminum alloys in liquid state, except for some information about the general laws of lithium influence on the oxidation of different metals stated in Shamrai [30], and there have been summary reports of difficulties in melting and casting of aluminum–lithium alloys because of their high aggressivity in liquid state.

In connection with this, the questions of melting and casting of ingots alloyed with lithium have assumed high urgency, and studying their interaction with the ambient atmosphere, as well as developing ways to protect these alloys during melting and casting from lithium loss, hydrogen saturation, and other metallic and non-metallic impurities, is required.

The oxidation rate of metals and alloys depends on several factors, primarily on alloy composition, the nature of the elements included in alloy composition, gas environment composition, temperature, and heating time [31,32].

Oxidation reactions of most metals and alloys are surface reactions. Therefore, the more the surface metal contacts with the environment, the greater the loss from oxidation.

Direct contact of the metal with the oxidative environment exists only in the initial moment of oxidation, and the oxidation proceeds through the oxide film thereafter.

Therefore, the oxidation rate of metal is often dependent on the characteristics of the oxide film.

The main characteristic that determines the protective properties of the oxide film is the Pilling–Bedworth ratio,  $\eta$ :

$$\eta = V_{\text{MemOn}}/V_{\text{Me}} \quad (2.1)$$

where

$V_{\text{MemOn}}$  is the volume of 1 oxide mole

$V_{\text{Me}}$  is the volume of 1 metal atom gram

If the ratio is equal to or greater than unity, then the continuity condition is followed, and the film is protective. If the ratio is less than unity, the oxide is not enough to cover the metal surface with continuous layer; hence, the film is loosened, and pores and cracks appear.

Most oxides formed on metals satisfy continuity conditions, except for alkali oxides and alkali earth metal oxides (Table 2.1).

Oxidation of metals is a complex process consisting of a number of steps [32]: metal ionization; diffusion of metal ions and electrons from the surface of the metal oxide section through the oxide film and the oxide–gas section; diffusion of oxygen molecules to the oxide surface; oxygen adsorption activation on the oxide surface; joining of electrons to form oxygen ions; diffusion of oxygen ions and atoms through the oxide film to the metal surface; and chemical reaction of metal with oxygen.

At high-temperature oxidation, when thick films are formed, diffusion of particles through these films is the slowest ongoing process. Therefore, the rate of ion diffusion determines the overall oxidation rate. The ionic radius of metals is considerably

**TABLE 2.1**  
**Some Characteristics of Metals and Their Oxides**

Metal	Melting Temperature (°C)	Free Surface Energy (mj)/cm <sup>2</sup>	Ionic Radius (Nm)	Atomic Radius (Nm)	Oxide	Standard Measurement of Oxide Energy Forming, Kcal/Mol Oxide	Volume Ratio	
							Own Metal	Aluminum
Al	660	860	0.057	0.143	Al <sub>2</sub> O <sub>3</sub>	210.2	1.42	1.42
Li	180	—	0.068	0.155	Li <sub>2</sub> O	400.0	0.58	0.75
Cu	1083	926	0.098	0.128	CuO	82	1.64	—
Zn	419.5	105	0.083	0.139	ZnO	—	—	—
Mg	650	728	0.074	0.160	MgO	143.7	0.81	1.09
Na	97.83	171	0.092	0.189	Na <sub>2</sub> O	—	—	—
Be	1286	—	0.031	0.160	BeO	14.1	1.68	0.82
V	1525	—	0.097	0.181	V <sub>2</sub> O <sub>3</sub>	152	1.39	—
Ca	850	246	0.106	0.197	CaO	151.9	—	—

smaller than the ionic radius of oxygen (Table 2.1); therefore, oxygen diffusion can be neglected [31], and it can be considered that the oxidation rate is determined by the diffusion of metal ions.

However, this applies to such cases when the formed oxide films on the metal surface are protective, that is, they prevent direct contact of liquid metal with the ambient atmosphere. In cases when the surface film do not form a continuous dense layer ( $\eta < 1$ ) and is not protective due to the presence of pores and cracks, the oxidizing gas penetrates relatively easily to the metal surface and metal drops go outside under the influence of capillary forces and are immediately oxidized thereafter. Consequently, when studying the oxidation process, it is necessary to deal with the issues of mechanism, rate of growth, and morphology of the oxide films.

In isothermal conditions, several oxidation time laws are found: linear, parabolic, logarithmic, and asymptotic [32].

Aluminum and some other components of aluminum melts are very chemically reactive and form stable compounds under the reaction with water vapor and air oxygen [32,33]. The most commonly occurring compound, aluminum oxide ( $\text{Al}_2\text{O}_3$ ; also termed alumina), is a very strong chemical compound with negligible minor vapor pressure dissociation ( $1013 \times 10^{-40}$  Pa at  $750^\circ\text{C}$ ); the combination heat of the reaction  $2\text{Al}_{(\text{TB})} + 1.5\text{O}_2 \rightarrow \text{Al}_2\text{O}_3$  is about 1680 kJ/mol [34].

Alumina has a number of structural modifications, the existence of which is determined by the temperature and composition of the environment:  $\gamma$ ,  $\delta$ ,  $\lambda$ . The only stable oxide modification is  $\lambda$ - $\text{Al}_2\text{O}_3$  (corundum) with an R-lattice and density of about  $4 \text{ g/cm}^3$  at room temperature. However, it is rarely found as it is formed when oxidation is at  $927^\circ\text{C}$  [32]. The most common alumina differs by amorphous structure and appears on the early stages of oxidation [31]. During slow heating, aluminum oxide in the  $\gamma$ -modification arises on the surface [34] and comprises water molecules, stabilizing the lattice of oxide in the  $\gamma$ -modification.

As a rule, the oxide film on the surface of solid aluminum is considerably hydrated, that is, it contains  $\text{Al}(\text{OH})_3$  and  $\text{AlOOH}$  modification hydroxides in addition to the main component  $\gamma$ - $\text{Al}_2\text{O}_3$  [31].

Aluminum oxide is a semiconductor and has electronic conductivity [32]. Oxide formation processes of this type fall into Wagner's ion-electron theory of high-temperature parabolic metal oxidation, which is characterized by the mass transfer of metal ions  $\text{Me}^{n+}$  and electrons  $n\bar{e}$  from the metal surface through the film in the direction of the oxidant. The movement of oxygen ions through the film is not practically produced [32].

Since the oxidation kinetics is also determined by the morphology film, it has protective properties on the aluminum as continuity condition is satisfied (Table 2.1).

The alloying elements and impurities in aluminum substantially affect the structure and properties of films formed on the metal surface. The influence character can be estimated by thermodynamic parameters determining the oxidation reaction of different metals.

The preferential oxidation of one or another element depends on its oxygen affinity and concentration or, more precisely, on the activity in the molten alloy at heating temperature. The oxygen affinity can be measured approximately by oxide

formation warmth under standard conditions, referred to as one atom gram of oxide (Table 2.1).

The kinetics of alloy oxidation is also determined by what elements the molten surface layers are enriched with. It is known [35] that the surface layers are concentrated with substances lowering the free energy, that is, surface-active substances. Surface activity is significantly dependent on the physical and chemical properties of elements and is defined by the properties of all the components in the molten surface [31,35]. Surface-active substances usually reduce the surface tension.

An element with a lower surface tension than aluminum reduces the surface tension of the molten surface proportionally to the logarithm of its concentration, and surfactant properties begin to appear. The surface tension of pure metals ( $\sigma$ ) (Table 2.2) linearly depends on temperature ( $t$ ):

$$\sigma = \sigma_0 + (t - t_{\text{melting}})d\sigma/dt, \quad (2.2)$$

where

$\sigma_0$  is the surface tension at  $t_{\text{melting}}$

The surface activity is determined by the size of the component and its atomic radius, atomic number, and electronic structure and is characterized by a generalized statistical moment [35]:

$$m^e = eZ \varphi(\eta)/R_{Me} \quad (2.3)$$

where

$Z$  is the element atomic number

$e$  is the electron charge

$R_{Me}$  is the atomic radius

$\varphi(\eta)$  is the dimensionless parameter

---

**TABLE 2.2**  
**Temperature Dependence of Surface Tension and**  
**Generalized Statistic Moments of Some Elements**

Element	$\sigma_0$ at $t_{\text{melting}}$ mN/m	$d\sigma/dt$ N/m	$m^e$
Al	870	-0.34	0.458
Li	395	-0.15	0.22
Na	195	-0.089	0.183
K	111	-0.062	0.106
Mg	559	-0.39	0.30
Ca	361	-0.10	0.19
Ba	224	-0.095	0.18

---

According to Zadumkin theory, the surface-active elements are those with ratios of  $m_p^e > m_n^e$ , where  $m_p^e$ ,  $m_n^e$  are generalized statistical moments of solvent and impurity.  $m^e$  values for metals are given in Table 2.2, from which it follows that alkali (K, Na, Li) and alkaline-earth elements (Ba, Sr, Ca) have the greatest surface activity.

A single criterion of surface activity is not established, but in the data shown in Table 2.2, the correlation observed between surface tension and energy of some structural and thermodynamic element parameters is quite satisfactory.

In all presented parameters (Table 2.2), lithium is more surface active than magnesium, which also has a high surface activity. Therefore, in the surface layer of the aluminum, molten lithium and magnesium will be present.

Copper concentration in the surface layer is lower than the average concentration in the alloy. Tests carried out in [36] have shown that copper does not affect the process of aluminum oxidation. This is confirmed by electron diffraction studies.

In binary aluminum–magnesium alloys added with even small quantities of magnesium, the oxidation is significantly higher than in pure aluminum and sharply increases at alloy magnesium content growth. At low magnesium content, the thick film of  $MgO \cdot Al_2O_3$  spinel is formed on the molten surface along with a loose film of magnesium oxide [37]. Increase in Mg content results in magnesium oxide composed film having no protective properties. Beryllium additives in the amount of hundredths of a percent reduce the aluminum alloy oxidation with high magnesium content (over 10%) almost 200 times. The standard changes of free energy of beryllium and magnesium oxide formation are the same, but beryllium, having smaller ion radius, is more mobile, which determines the higher concentration of beryllium in the surface layer. This provides simultaneous oxidation of magnesium and beryllium. As shown by electron diffraction studies [38], at 0.005%–0.05% beryllium content in the alloy with 5% of magnesium, the heterogeneous film is formed consisting of a magnesium and beryllium oxide mixture. It is considered that mechanism of protection of aluminum–magnesium alloys by beryllium is mechanical healing by beryllium oxide of oxide film discontinuities consisting of magnesium oxide [37,38].

According to Wagner's theory, it is possible that the positive effect of beryllium in the oxidation process is associated with the fact that, having low conductivity, beryllium oxide should reduce the diffusion rate of lithium through oxides [32].

The comparison of lithium and magnesium characteristics, shown in Table 2.2, justifies that in aluminum–lithium–magnesium base alloys, both elements will influence the alloy oxidation process since they are surface-active substances, and consequently, the molten surface layer consists of the ion mixture of these elements. Being present together in the molten surface, these two surface-active substances mutually reduce activity [39]. However, lithium plays the leading role.

In accordance with the Langmuir theory, lithium forms a monomolecular layer in the alloys of aluminum–copper–lithium-based systems and it remains in contact with the atmosphere.

Based on the carried-out analysis of characteristics in Tables 2.1 and 2.2 and the positive experience of beryllium use as a protective additive in alloys with high magnesium content, it became interesting to test beryllium and yttrium having  $\eta > 1$  as a protective additive to alloys with high lithium content.

## 2.2 OXIDATION KINETICS AND MECHANISM OF PROTECTIVE ALLOYING OF ALUMINUM–LITHIUM ALLOYS

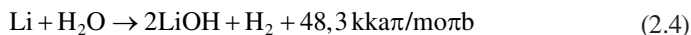
### 2.2.1 Al–Cu–Li SYSTEM ALLOY

The oxidation kinetics of Al–Cu–Li system was studied on 1230 alloys (international equivalent of 2020) [44]. On the molten bath surface of 1230 alloy right after lithium introduction, the matte film is formed, which thickens, becomes loose, and cracks along with increase in holding time. Open metal is covered immediately with matte film again. The results of the chemical analysis, shown in Figure 2.1, demonstrate that 1230 alloy is oxidized in accordance with linear law and that the process intensity increases with the increase of melt temperature [40,41].

The investigation of film formed on the melt after 120 min holding showed that it was not uniform in thickness but consisted of two layers. The top layer was white and the lower layer adjacent to the melt was light gray.

X-ray crystal phase analysis carried out after layered film separation showed that the top layer consisted of lithium phases—lithium oxide ( $\text{Li}_2\text{O}$ ) and lithium hydroxide ( $\text{LiOH}$ ); the lower layer consisted of transition alumina ( $\gamma\text{-Al}_2\text{O}_3$ ) and lithium oxide ( $\text{Li}_2\text{O}$ ).

Lithium hydroxide can be a product of either the direct reaction of lithium with



water vapor or the secondary reaction of lithium oxide with water vapor.

The study [42] conducted with 2090 alloy shows the formation of a film consisting of  $\text{Li}_2\text{O}$ ,  $\text{Li}_2\text{CO}_3$ , and  $\text{LiAlO}_2$  at samples heated at temperatures ranging from  $200^\circ\text{C}$  to  $550^\circ\text{C}$ .

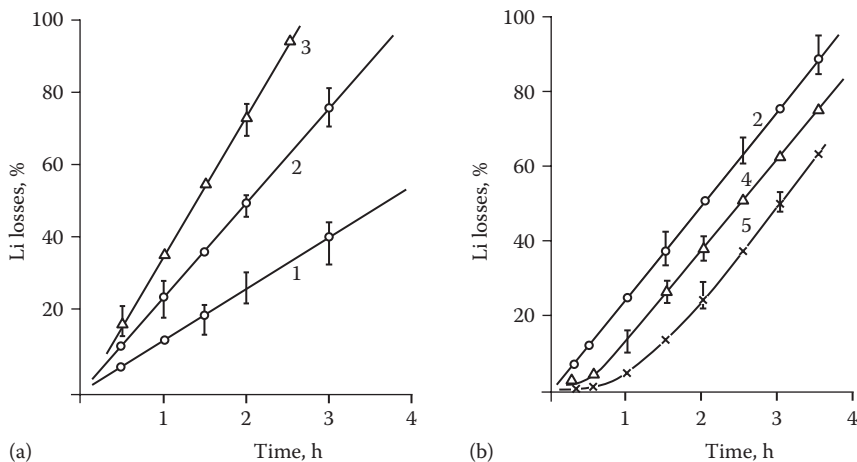


**FIGURE 2.1** Kinetics of lithium burnout from 1230 alloy: (a) without protection of bath level at temperatures: 1— $680^\circ\text{C}$ ; 2— $700^\circ\text{C}$ ; 3— $720^\circ\text{C}$  and (b) with beryllium: 4—0.02%; 5—0.26%.

Beryllium doping in 1230 alloys in amounts of 0.02%, 0.07%, 0.10%, 0.20%, and 0.26% do not provide the effect of long-term protection (Figure 2.1). At concentrations greater than 0.10%, there is only a short-term effect of alloy oxidation (Figure 2.1, curve 5). During 5–6 min, the metal surface stays shiny, which corresponds to the flat section of the specified diagram. Then, the metal surface bounces by light gray matte film, which thickens along with increase in holding time, darkens, and begins to explode and burst. The mechanism of short-term protection can be attributed probably to the reciprocal activity decrease of two surfactants [43], which delays the lithium output to the molten surface. This explanation can be considered reliable since additional phases, including beryllium, were not detected in the film during x-ray diffraction analysis [43,44]. Due to lithium deficiency, the poorer compound is produced—lithium hydroxide having  $\eta$  greater than one.

Based on the specified data, it follows that beryllium being present in significant amounts in 1230 alloy gives only short-term protection of the alloy and is not recommended for long-term alloy protection from oxidation during melting.

### 2.2.2 Al–Mg–Li SYSTEM ALLOY

The kinetics of Al–Mg–Li system alloy oxidation was investigated with 1420 alloy. Peculiarity of 1420 alloy is the simultaneous presence of two surface-active elements (magnesium and lithium) in much greater quantities than in AMg6 and 1230 (Table 2.3).

Taking into account the results of protective alloying of 1230, the introduction of 0.15%–0.25% beryllium and yttrium in 1420 alloy was tested. A loose film constantly increasing in thickness, initially white, and turns dark gray with lots of cracks after a holding time of 120 min, is formed in alloy without any addition of protective elements. Such film does not protect the alloy from oxidation, which proceeds in accordance with linear law, starting after 15–30 min of storage (Figure 2.2).

Having 0.2% Be during the first 5–7 min after lithium injection, the elastic shiny film is formed, which is separated with difficulty from the melt surface and stretches after the sampler. At further molten storage, the film becomes matte and brittle and

**TABLE 2.3**  
**Surface-Active Elements Content in Some**  
**Aluminum Alloys**

Alloy	Element Content at.(%)		
	Li	Mg	Total
1420	8.8 (2.2)	5.5 (5.0)	14.3
AMg6	—	6.6 (6.0)	6.6
1230	4.8 (1.2)	—	4.8

*Note:* Percentage weight element content in parentheses.

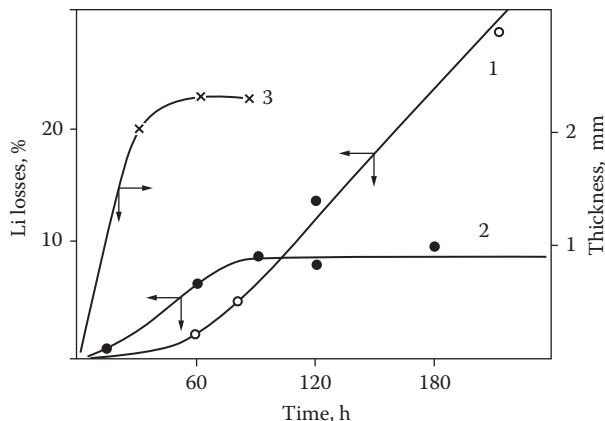


**FIGURE 2.2** Kinetics of lithium burnout from 1420 alloy without beryllium additives (1) and with 0.2% beryllium addition (2), also with thickness of surface film on the alloy with 0.2% of beryllium (3).

its thickness increases rapidly (Figure 2.2), and in the same period on the lithium burnout kinetic curve, a steep part is observed, which increases the oxidation rate. After 30–45 min, the film thickness growth rate slows down, and by 60 min, the thickness growth is no longer observed, the film color turns into gray, and dark brown spots are visible. The kinetic burnout curves show the process rate reduction after 60 min of storage, and after 80 min, oxidation practically stops.

At 0.2% yttrium introduction, the dense brittle film is formed, the thickness of which varies slightly and strength rises along with increase in molten holding time. During melt exposure, the oxidation reactions occur, resulting in no additive alloy and the formation of  $\chi$ - $\text{Al}_2\text{O}_3$  and  $\text{Li}_2\text{O}$  oxides.

Along with high speed oxidation, the secondary moisture interaction reaction and carbon dioxide reaction occur resulting in after 1–3 min the  $\text{LiOH}$  hydroxide and  $\text{Li}_2\text{CO}_3$  carbonate formation on the molten surface. Hydroxide at holding temperature stays in the molten state ( $T_{\text{melting}} = 462^\circ\text{C}$ ), and carbonate is close to the molten state ( $T_{\text{melting}} = 732^\circ\text{C}$ ) (Table 2.4).

Calculation of the Pilling–Bedworth ratio for these phases showed that they must have protective properties in liquid aluminum (Table 2.4) [43].

It is experimentally confirmed that, kinetically, during the first minutes of storage, when the reaction rate of  $\text{Li}_2\text{O}$  formation slightly exceeds the reaction rate of  $\text{Li}_2\text{CO}_3$  and  $\text{LiOH}$  formation (Table 2.5), lithium burning in the molten state proceeds weakly, which is indicated by a plateau (Figure 2.2, curve 1).

In the alloy with beryllium,  $\text{Li}_2\text{O}$  oxide in its pure form is absent; it is consumed for the formation of  $\text{Li}_2\text{CO}_3$  and  $\text{LiOH}$  mixtures (Table 2.6). On the beryllium alloy oxidation kinetic curve, the presence of a plateau at short holding time is explained by the presence of these phases.

$\gamma$ - $\text{LiAlO}_2$  oxide is formed at temperatures above  $600^\circ\text{C}$  and at normal pressure in 3–5 min after lithium introduction into the molten state without additives and with

**TABLE 2.4**  
**Physical Characteristics of Compounds Formed on the 1420 Molten Surface**

Compound	Crystal Lattice	Melting Temperature (°C)	Density (kg/m <sup>3</sup> )	Molar Volume (cm <sup>3</sup> )	Volume Ratio <sup>a</sup>
Li <sub>2</sub> O	FCC	2000	2013	15	0.75
LiOH	Tetragonal	462	1460	16.4	1.26
Li <sub>2</sub> CO <sub>3</sub>	Monocrystalline	618 (732)	2110	37	1.42
γ-LiAlO <sub>2</sub>	Tetragonal	—	2610	25.0	1.26
MgO	FCC	3073	3650	11.25	1.09
BeO	Hexagonal	2843	3030	8.25	—

<sup>a</sup> Calculated relative to alloy.

**TABLE 2.5**  
**Kinetics of 1420 Molten Surface Films Phase Composition Changes without the Bath Surface Protection**

Time <sup>a</sup> (min)	Phase Compounds <sup>b</sup>							
	Al	χ-Al <sub>2</sub> O <sub>3</sub>	Li <sub>2</sub> O	—	—	—	—	—
1	Al	χ-Al <sub>2</sub> O <sub>3</sub>	Li <sub>2</sub> O	—	—	—	—	—
2	Al	χ-Al <sub>2</sub> O <sub>3</sub>	Li <sub>2</sub> O	LiOH	—	—	—	—
3	Al	χ-Al <sub>2</sub> O <sub>3</sub>	Li <sub>2</sub> O	LiOH	Li <sub>2</sub> CO <sub>3</sub>	γ-LiAlO <sub>2</sub>	MgO	—
4	Al	χ-Al <sub>2</sub> O <sub>3</sub>	Li <sub>2</sub> O	LiOH	Li <sub>2</sub> CO <sub>3</sub>	γ-LiAlO <sub>2</sub>	MgO	—
5	Al	χ-Al <sub>2</sub> O <sub>3</sub>	Li <sub>2</sub> O	LiOH	Li <sub>2</sub> CO <sub>3</sub>	γ-LiAlO <sub>2</sub>	MgO	—
6	Al	χ-Al <sub>2</sub> O <sub>3</sub>	Li <sub>2</sub> O	LiOH	Li <sub>2</sub> CO <sub>3</sub>	γ-LiAlO <sub>2</sub>	MgO	LiH
10	Al	χ-Al <sub>2</sub> O <sub>3</sub>	Li <sub>2</sub> O	LiOH	Li <sub>2</sub> CO <sub>3</sub>	γ-LiAlO <sub>2</sub>	MgO	LiH
15	Al	χ-Al <sub>2</sub> O <sub>3</sub>	Li <sub>2</sub> O	LiOH	Li <sub>2</sub> CO <sub>3</sub>	γ-LiAlO <sub>2</sub>	MgO	LiH
120	Al	χ-Al <sub>2</sub> O <sub>3</sub>	Li <sub>2</sub> O	LiOH	Li <sub>2</sub> CO <sub>3</sub>	γ-LiAlO <sub>2</sub>	MgO	—

<sup>a</sup> Time after lithium introduction.

<sup>b</sup> The phases are located in the order of their quantity reduction in the corresponding film.

beryllium, and in 1 min after lithium introduction with yttrium additives on the film surface composite.

γ-LiAlO<sub>2</sub> oxide, like many oxides with A<sup>+1</sup>B<sup>+3</sup>O<sub>2</sub> formula, has a tetragonal structure. Its lattice periods are a = 5.169 Å and c = 6.268 Å. However, unlike other oxides, such as LiFeO and LiZnO, which are similar to NaCl structure and in which the cations are coordinated octahedrally, except for γ-LiAlO<sub>2</sub>, lithium and aluminum are coordinated tetrahedrally. The Pilling–Bedworth ratio for (η) oxide calculated on the density data basis [45] equals to 1.26 (Table 2.4).

During half-hour storage at 720°C, the surface layers of 1420 alloy without additives consist of phase mixture with different structures and properties. At longer-term holding, when the lithium and magnesium oxidation is simultaneous, the Li<sub>2</sub>O

**TABLE 2.6**  
**Kinetics of 1420 Molten Surface Films Phase Composition Changes with 0.2% Beryllium Addition**

Time <sup>a</sup> (min)	Film Color	Phase Compound <sup>b</sup>								
		Al	MgO	Li <sub>2</sub> CO <sub>3</sub>	LiOH	Li <sub>2</sub> CO <sub>3</sub>	γ-LiAlO <sub>2</sub>	MgAl <sub>2</sub> O <sub>4</sub>	BeAl <sub>2</sub> O <sub>4</sub>	BeO
1	White	Al	MgO	Li <sub>2</sub> CO <sub>3</sub>	LiOH					
2	White	Al	MgO	LiOH	Li <sub>2</sub> CO <sub>3</sub>					
3	White	Al	MgO	LiOH	Li <sub>2</sub> CO <sub>3</sub>					
4	White-gray	Al	MgO	LiOH	Li <sub>2</sub> CO <sub>3</sub>					
5	White	Al	MgO	LiOH	Li <sub>2</sub> CO <sub>3</sub>	γ-LiAlO <sub>2</sub>				
	Gray	Al	MgO	LiOH	Li <sub>2</sub> CO <sub>3</sub>	γ-LiAlO <sub>2</sub>				
6	White-gray	Al	MgO	LiOH	Li <sub>2</sub> CO <sub>3</sub>	γ-LiAlO <sub>2</sub>	MgAl <sub>2</sub> O <sub>4</sub>			
10	Black	Al	MgO	Γ-LiAlO <sub>2</sub>	MgAl <sub>2</sub> O <sub>4</sub>	BeAl <sub>2</sub> O <sub>4</sub>				
15	White-gray	Al	MgO	Li <sub>2</sub> O	LiOH	Li <sub>2</sub> CO <sub>3</sub>	γ-LiAlO <sub>2</sub>			
	Black	Al	MgO	LiOH	Li <sub>2</sub> CO <sub>3</sub>	γ-LiAlO <sub>2</sub>	MgAl <sub>2</sub> O <sub>4</sub>	BeAl <sub>2</sub> O <sub>4</sub>	BeO	
20	Black	Al	MgO	LiOH	Li <sub>2</sub> CO <sub>3</sub>	MgAl <sub>2</sub> O <sub>4</sub>	BeAl <sub>2</sub> O <sub>4</sub>	γ-LiAlO <sub>2</sub>	BeO	

<sup>a</sup> Time after lithium introduction.

<sup>b</sup> The phases are located in the order of their quantity reduction in the corresponding film.

and MgO phase quantity significantly increases, which leads to the formation of loose film, providing no protection for 1420 alloy without additives from continuous oxidation. As shown in Table 2.5, the predominant phase at long-term holding is lithium oxide.

When studying the kinetics of Al–Li–Cu–Mg–Zr system alloy oxidation [46,47], the researchers found out the Li<sub>2</sub>CO<sub>3</sub>, α-Li<sub>5</sub>AlO<sub>2</sub>, and γ-LiAlO<sub>2</sub> phases formation at 500°C during a holding time of 160 min.

With the presence of 0.2% beryllium, the Li<sub>2</sub>O lithium oxide appearance in the film is accompanied by an increase in oxidation rate, which corresponds to a steep section on the kinetic curve. However, beginning with 8 min, the separate parts of the molten surface are covered with dark-gray film comprising phases with protective properties—MgAl<sub>2</sub>O<sub>4</sub> and BeAl<sub>2</sub>O<sub>4</sub>—having η greater than one (Table 2.6), but the number of these phases is not sufficient to stop the burning of lithium. Within the 30–45 min holding range, there are two competing processes on the surface: Li<sub>2</sub>O formation and beryllium and magnesium complex oxides formation, and therefore, the surface area occupied by MgAl<sub>2</sub>O<sub>4</sub> and BeAl<sub>2</sub>O<sub>4</sub> determines the speed of lithium burning and not the film thickness. After 30–45 min, the surface film growth rate of the complex composition on the molten with beryllium slows down (Figure 2.2). This indicates that the amount of lithium-containing phases becomes constant. Lithium burning process stops only after 90 min when the entire molten surface is covered with dark film of complex oxide mixtures.

The protective properties of γ-LiAlO<sub>2</sub> oxide are revealed most completely in melting alloys with yttrium (Table 2.7). The amount of lithium carbonate after a holding time of 2 h remains constant, while the number of γ-LiAlO<sub>2</sub> oxide in